1-24-94
E-8253

An Investigation of Magnetic Field Effects on Plume Density and Temperature Profiles of an Applied-Field MPD Thruster

S. Ray Bullock
National Aeronautics and Space Administration
Lewis Research Center
Cleveland, Ohio

and

R.M. Myers
Sverdrup Technology, Inc.
Lewis Research Center Group
Brook Park, Ohio

NASA

An Investigation of Magnetic Field Effects on Plume Density and Temperature Profiles of an Applied-Field MPD Thruster

S. Ray Bullock
National Aeronautics and Space Administration
Lewis Research Center
Cleveland, Ohio 44135

and

R.M. Myers
Sverdrup Technology, Inc.
Lewis Research Center Group
Brook Park, Ohio 44142

Abstract

Applied-field magnetoplasmadynamic (MPD) thruster performance is below levels required for primary propulsion missions. While MPD thruster performance has been found to increase with the magnitude of the applied-field strength, there is currently little understanding of the impact of applied-field shape on thruster performance. This paper presents the results of a study in which a single applied-field thruster was operated using three solenoidal magnets with diameters of 12.7, 15.2, and 30.4-cm. Thruster voltage and anode power deposition were measured for each applied-field shape over a range of field strengths. Plume electron number density and temperature distributions were measured using a Langmuir probe in an effort to determine the effect of field shape on plume confinement by the diverging magnetic-field for each of the three magnetic field shapes. Results show that the dependence of the measured thruster characteristics on field shape were non-monotonic and that the field shape had a significant effect on the plume density and temperature profiles.

Nomenclature

a	probe arm length, cm	n_e	electron number density, m^{-3}
A_p	probe area, m^2	n_i	ion number density, m^{-3}
A_s	sheath surface area, m^2	P_A	anode power, kW
B	magnetic field, T	P_T	total power, kW
c_p	specific heat of water, kJ/kgK	R	probe radius, m
e	electron charge, C	r	radial location of probe, cm
E	electric field, V/m	r_{Le}	electron Larmor radius, m
I_e	probe electron current, A	t	time, s
I_+	probe ion current, A	ΔT	temperature change, C
j_e	electron current density, A/m^2	T_e	electron temperature, K
j_i	ion current density, A/m^2	T_i	ion temperature, K
j_i^*	normalized ion current	v	electron thermal velocity, m/s
J	thruster current, A	v_p	probe velocity, cm/s
k	Boltzmann's constant,1.38×10^{-23} J/K	V	thruster voltage, V
m	mass flow rate, kg/s	V_p	plasma potential, V
m_e	electron mass, kg	z	axial distance, cm
m_i	ion mass, kg	Z	charge number

1

ξ_p	R/λ_D
ε	T_i/T_e
Γ	ion mass flux, kg/s
λ_D	Debye length, m
Φ	non-dimensionalized mass flux
σ_0	permittivity of free space

Introduction

MPD thrusters may become competitive with chemical and other electric propulsion technologies for future primary electric propulsion applications such as low-power orbit raising and manuevering missions. Characterized by high specific impulse, high thrust density, and system simplicity, MPD thrusters will be suitable for these types of missions if the power-to-thrust conversion efficiency can be increased to over 40%.[1,2] However, current thruster efficiencies are below 30% and research efforts are focused on increasing this value.

Figure 1 shows a cutaway schematic of an applied-field MPD thruster. The propellant is injected through the backplate and ionized in the annular region between electrodes. The charged particles are then accelerated by the Lorentz forces generated by the interaction of the discharge current with both the self-induced and applied magnetic-fields. While the self-field acceleration mechanisms are present in both the self-field and the applied-field MPD thrusters, the addition of an applied-field results in both the addition of azimuthal kinetic energy to the propellant flow, which can be converted to axial kinetic energy,[3] and in the formation of a magnetic nozzle, which can convert thermal energy to axial kinetic energy.[4] The magnetic nozzle functions by confining the plasma within magnetic flux tubes during the expansion process. It is not known which of these phenomena dominate the acceleration process in applied-field thrusters. Note, however, that if the plasma in the nozzle were to rigidly follow the magnetic flux tubes, thrust would be lost because the field lines must ultimately close. Theoretical studies have indicated that the shape of the applied-field plays a role in establishing the efficiency of the plasma separation and magnetic-nozzle processes.[3-7]

Previous studies have shown that MPD thruster performance improves with increasing power level and applied-magnetic field strength.[2,8] Steady-state applied-field thrusters have consistently shown performance levels higher than those of self-field devices.[9-11] Although there has been a considerable amount of research into understanding the electrode and internal plasma losses,[12-14] little effort has been expended in examining the losses associated with the plasma confinement by the applied-magnetic field lines.

This paper presents preliminary results from an effort to identify the effects of the applied magnetic-field shape on the thruster discharge voltage, anode power-fraction, and plume electron density and temperature profiles. A qualitative evaluation of plasma confinement by the applied magnetic-field is also presented.

MPD Thruster System

The MPD thruster cathode was 0.64-cm in radius, 7.6-cm-long, and made from 2% thoriated tungsten. The anode was a coaxial 7.6-cm-long copper cylinder of inner radius 2.54-cm. As shown schematically in Figure 1, both electrodes were water-cooled. The anode was cooled using azimuthal passages in the wall. The cathode was cooled at the base by a water-cooled copper cathode clamp. Propellant was injected through a boron nitride backplate via a 0.16-cm-wide annulus surrounding the cathode and twenty-four 0.16-cm diameter holes at the mid-radius between the cathode and anode. All gas seals were made using 0.05-cm-thick graphite gaskets.

The thruster was tested with three different water-cooled magnets with inner diameters of 12.7, 15.2, and 30.4-cm. The largest diameter magnet was 17.8-cm-long and consisted of 45 turns of 1.27-cm diameter copper tubing. The 15.2-cm diameter magnet was approximately the same length, used the same size tubing, and had the same number of turns as the 30.4-cm diameter magnet. The 12.7-cm diameter magnet consisted of 24 turns of 1.27-cm diameter tubing. Each magnet was aligned flush with the thruster's exit plane during testing. The magnets were calibrated using a Hall probe to measure the magnetic field strength at five azimuthal locations on the thruster exit plane as the magnet current was varied. Iron-filing maps were made for all geometries to determine the magnetic-field shape. The magnetic field line originating at a radius of 2.1-cm from the centerline at the exit plane was chosen to define a magnetic flux tube used for plasma confinement studies. This initial radius was chosen because it was located between the electrodes and it was the easiest to trace for all magnet geometries. Figure 2 shows the flux tube radius versus axial position for all three geometries. As expected, the flux tube for the smallest magnet diverged most rapidly, with the flux tube radius increasing from 2.1-cm to 7-cm at an axial distance of

14-cm from the thruster exit plane. The expansion area ratios for the three magnets corresponding to the flux tube radii shown in Figure 2 are 11, 5, and 3, respectively, at an axial distance of 14-cm from the thruster exit plane.

Test Facility

All tests were conducted using a 1-m diameter by 1-m-long test port which is connected to a 4.5-m diameter by 18.3-m long vacuum tank. The thruster was mounted on a platform which was extended into the main tank through a 1-m diameter gate valve using a set of door slides. The chamber was pumped by a 41 m^2 helium cryopanel system. The cryopump provided a pumping speed of 2×10^5 l/s at the port with argon propellant.[15] The tank pressure was maintained below 0.026 Pa during testing with a nominal argon flow rate of 0.10 g/s. Two ionization gauges located on opposite ends of the tank were used to monitor the tank pressure.

The MPD thruster was powered by a series-parallel ladder network of six welding supplies with an output capability of 3000 A at 130 V. The applied magnetic field coil was powered by a single welding supply capable of providing up to 1500 A. All welding supplies were isolated from ground. Thruster voltages and currents were recorded continuously by display meters and the computer-based data acquisition system. The voltage and current measurement uncertainties were +/-0.5 V and 5.0 A, respectively. The thruster and magnet were water-cooled by two closed loop heat exchangers, each providing flow rates up to 0.5 l/s. The water flow rate was measured using turbine flow meters which were calibrated at regular intervals during testing. The propellant was provided by two mass flow controllers capable of 15 SLM. These were calibrated for argon. Both controllers were calibrated at regular intervals during testing and the deviation between calibrations was never more than 1%. The mass flow rate was accurate to +/- 0.005 g/s.

Diagnostics

The anode power was measured calorimetrically using chromel-alumel thermocouples placed in the cooling water inlet and outlet lines. The anode power was calculated using:

$$P_A = mc_p \, \Delta T \tag{1}$$

The accuracy of the water temperature measurements was +/- 0.5 Celsius. The anode power-fraction was calculated by dividing P_A by the total input power to the thruster. Magnet power was not used in this power balance.

The plume electron density and temperatures were measured using a single Langmuir probe. The probe was a 0.15-mm diameter, 0.7-cm-long, tungsten wire mounted in a 0.20-cm outer diameter, 3.5-cm-long ceramic cylinder. The probe was installed on a 38-cm long water-cooled stainless steel arm as shown in Figure 3. As shown in the figure, the probe rested horizontally beneath the thruster between passes through the plume. The probe arm length and axis of rotation were chosen so that the probe passed through the center of the plume as shown in Figure 4. The probe motion system (PMS) used a DC-stepper motor-driven linear actuator to provide the axial motion and a 30 V DC rotary motor to sweep the probe through the plume at approximately 60 cm/s. The PMS and data acquisition were controlled by a computer based measurement and control system.

The Langmuir probe was biased with respect to the vacuum tank wall using a bipolar amplifier driven by a function generator as shown in Figure 5. The function generator provided a 150-Hz triangle wave which ramped between +5 and -15 volts. This frequency and probe rotation speed provided a complete probe characteristic every 2-mm across the probe path. Probe current and voltage data were collected continuously at 150-kHz resulting in 301 points per Langmuir probe characteristic. Plasma properties were obtained at a minimum of three axial distances from the exit plane for all geometries. Figure 4 shows the geometry of the probe with respect to the MPD thruster. The radial location of the probe was calculated from the law of cosines using:

$$r = a[\, 2(1-\cos(v_p t/a)) \,]^{1/2} \tag{2}$$

where a is the length of the probe arm and v_p is the probe velocity.

Because of the wide range in plasma conditions across the plume, the Langmuir probe data were analyzed using both simple thin-sheath probe theory and the more general theory developed by Laframboise.[16] This was done to establish the limits of validity for thin-sheath theory. To begin the data reduction, a voltage ramp was identified for analysis. Figure 6 shows a typical probe trace after subtraction of the average ion saturation current from the entire trace. The data shown were obtained using the 15.2-cm diameter magnet at a

3

field strength of 0.04 Tesla. This plot illustrates the curve fit used to determine the electron temperature from the electron-retarding region. As indicated in Figure 6, it was common for the linear region to extend over a current range of nearly two orders of magnitude. The electron temperature was obtained from a least -squares curve fit of $\ln(-I_e)$ versus the probe potential across the electron-retarding region, which is linear with a slope of e/kT_e. Uncertainties associated with this analysis were generally due to an inaccurate curve fit for the electron temperature. Uncertainties can be minimized by examining the plot and adjusting the number of points in the region until the best fit is obtained. Once the temperature was obtained, it was used with the electron saturation current to calculate the electron number density from:

$$n_e = j_e /[ZeA_p(kT_e/2\pi m_e)^{1/2}] \qquad (3)$$

In Laframboise' model the value of r_p/λ_D and T_i/T_e must be known in order to use the fitting formulas needed to calculate the electron and ion densities.[16] For all data presented, the ratio of T_i/T_e was assumed to be 1. The sensitivity of the analysis to this assumption was tested by increasing and decreasing T_i/T_e by a factor of 10. The densities deviated by less than 20% from those calculated assuming this ratio was 1. Since r_p/λ_D depends on T_e and n_e, an iterative process was used in the data reduction. The electron temperature was calculated from the electron-retarding region as described in the simple probe model above. The fitting formula used to calculate the densitiy was given by: [16]

$$j_i^* \xi_p^2 = (R^2/\sigma_0)(2\pi m_i /e)^{1/2}(e/kT_e)^{3/2}(I_+/A_p) \qquad (4)$$

where j_i^* is the ion current normalized with respect to the random ion current evaluated at the electron temperature. It should be noted that π was mistakenly omitted in Reference 16. Although Laframboise' theory permits electron density calculations from both the electron and ion saturation regions, the densities calculated from the electron saturation region were used for these analysis because this region, in general, could be measured with the highest accuracy and should be less sensitiive to changes in probe orientation with respect to the flow velocity.

A potential problem with the Langmuir probe analysis arises from the presence of the magnetic fields. To neglect magnetic-field effects, the following condition must be met:[17]

$$r_{Le}/R \gg 1 \qquad (5)$$

For the highest magnetic-field strength used in these tests, 0.14 T, this ratio was 0.3 at the exit plane. The ratios of Equation 5 on the centerline at the two extreme axial distances for which data was obtained, 4 and 19-cm, were 0.45 and 1.7, respectively. The ratios for the smallest magnetic-field strength, 0.04 T, at the same locations were 1 and 6 at axial stations of 4 and 19-cm, respectively. For this range of r_{Le}/r_p the electron saturation current is clearly being suppressed, so that the measured electron density results are likely lower than the true values.[17] The uncertain nature of the theories describing this phenomena precluded any quantitative analysis.

Results and Discussion

Thruster Characteristics

The MPD thruster was operated at a discharge current of 1000 A, an argon flow rate of 0.1 g/s, and with applied-magnetic field strengths ranging from 0.03-0.14 Tesla. The reference axial magnetic-field strength was measured on the centerline at the exit plane. The thruster was ignited at the lowest field strength and allowed to stabilize for several minutes before the thruster and plume characteristics were recorded. The magnetic-field strength was then increased to the next value and allowed to stabilize before taking the next data set.

Figure 7 shows a plot of the discharge voltage versus applied-field strength for all three magnet geometries. For all cases the discharge voltage increased nearly linearly with increasing field strength. The thruster conditions for the 15.2 and 30.4-cm diameter magnets were very stable and reproducible. When testing with the small, 12.7-cm diameter magnet, there was considerable hysteresis in the thruster conditions, which accounts for the large scatter in the data for this geometry. The 15.2-cm magnet geometry yielded the highest discharge voltage, 55 V, at an applied-field strength of 0.14 Tesla. The results using the 15.2-cm diameter magnet are consistent with a previous investigation of geometric effects, in which a similar anode-to-magnet ratio was used.[8] The lowest discharge voltage, 21.5 V, was obtained using the 30.4-cm magnet geometry at 0.04 Tesla. The non-monotonic

4

behavior of the discharge voltage as a function of magnet radius shown in Figure 7 suggests that the applied-field shape can be optimized. The reasons for the non-monotonic behavior are not clear and the results are complicated by hysteresis in the operating conditions.

In Figure 8a, the anode-power is shown for all three geometries. For all three magnet diameters the anode-power increased monotonically with increasing field strength. As observed with the discharge voltage, the results for the 15.2 and 30.4-cm diameter magnets were stable and reproducible, but were not so when using the 12.7-cm diameter magnet. For this magnet configuration, the measurement fluctuations were particularly evident at 0.05 and 0.10 Tesla. While the scatter in the results for the 12.7-cm diameter magnet makes it impossible to conclusively identify trends, the lower anode power was clearly obtained with the 30.4-cm diameter magnet. The non-monotonic behavior suggests that there is an optimum field shape for which the anode-power can be minimized.

The thruster and anode power measurements were combined to calculate the anode power-fraction which is plotted versus the applied-field strength in Figure 8b. For all geometries there was considerable scatter in the results at the lowest field strengths. The anode power-fraction generally decreased with increasing field strength, though there was clear evidence of a plateau for field strengths between 0.05 and 0.10 Tesla. The highest anode power-fraction was about 77% at an applied-field strength of 0.03 Tesla using the 12.7-cm magnet geometry. For both the 15.2 and 30.4-cm magnet geometries, the highest anode power fraction occured at the lowest field strength. These findings are generally consistent with earlier studies.[11] The lowest power fraction was about 66% for the 15.2-cm magnet geometry at a field strength of 0.14 Tesla.

Plume Characteristics

Typical measured electron density profiles for the three magnet geometries are shown in Figures 9-11. The magnitude of the centerline electron density decreased and the width of the plume increased with increasing axial distance for all cases. As shown in Figure 9, an electron density of 3×10^{18} m^{-3} was obtained using the 12.7-cm magnet geometry at a field strength of 0.14 Tesla. Figure 10 shows the results for the 15.2-cm magnet at a field strength of 0.04 Tesla, which yielded the highest electron density of 4×10^{18} m^{-3}. The lowest value, 2×10^{18} m^{-3}, was obtained using the 30.4-cm magnet geometry at a field strength of 0.04 Tesla, as shown in Figure 11. Comparing Figures 10 and 11 it can be seen that the centerline electron density decreased with increasing magnet diameter.

Figures 12-14 show electron temperature measurements for all three geometries at three axial locations. While the scatter in the measurements was large, the electron temperature clearly decreased with increasing axial distance for all cases. The radial temperature gradients were too small to detect. As illustrated in Figure 12, the highest electron temperature, 50,000 K was observed using the 12.7-cm diameter magnet at 0.14 Tesla. From Figures 13 and 14 it is seen that both the 15.2 and 30.4-cm diameter magnets yielded centerline electron temperatures of about 35, 000 K at the reduced field strength of 0.04 Tesla. While not shown in the figures, testing revealed that the centerline electron temperatures increased as the magnetic field strength was increased. The highest temperatures measured using the 15.2 and 30.4-cm diameter magnets were 45,000 and 35,000 K at a field strength of 0.14 Tesla, respectively, which are close to the values shown in Figure 12 for the 12.7 cm magnet. These findings suggest that the shape of the field plays a small role in determining the electron temperature.

Plasma Confinement Studies

The plume measurements described above were used to qualitatively examine the plasma confinement within the applied magnetic field lines. This was done by calculating the ionized mass flux enclosed in the flux tubes defined in Figure 2 at each axial location that electron density measurements were taken using the relation:

$$\Gamma(z_k) = 2\pi m_i \sum_j n_j(r) v_i(r) r_j \Delta r \qquad (6)$$

where the indices j and k refer to radial and axial locations, respectively, and a quasi-neutral, fully ionized plasma was assumed. The plasma was assumed to be quasi-neutral since only electron density measurements were made. The plasma velocity was calculated from thrust measurements made by Myers[18] and assuming a constant velocity throughout the plume. The flux was non-dimensionalized by dividing $\Gamma(z_k)$ by the enclosed flux calculated at z=4 cm using:

$$\Phi(z) = \Gamma(z_k)/\Gamma(4 \text{ cm}) \qquad (7)$$

5

and plotted versus the axial distance. The results for the magnet geometries are shown in Figures 15 and 16 for low and high applied-field strengths, respectively. No results are presented for the 12.7 cm magnet at the lowest field strength because the thruster was unstable. The results show that the enclosed ionized mass flux generally increased with axial distance although a decrease was observed at one axial location with the 15.2-cm diameter magnet. In addition, comparing the results for the three magnet geometries did not reveal any clear trends in the behavior of the enclosed mass flux.

The observed increase in Φ with axial distance may be due to two phenomena. First, because the initial flux tube radius of 2.1-cm is within the anode radius, mass from near the anode but initially outside the flux tube could be entering the flux tube as the field diverges. This phenomena would indicate that the plasma is not trapped within the field lines. Second, the true flow velocity may actually be decreasing with axial distance in contrast to the assumed constant flow velocity. The decrease in flow velocity is not inconsistent with theoretical predictions by Moses,[19] who showed that substantial momentum loss could result from resistive detachment of the plasma from the applied field. Note that in no case did Φ decrease continuously with axial distance, a result which would have indicated that the plasma density was decreasing more rapidly than the field lines were diverging. More detailed diagnostics with velocity probes are required to better document the ionized flow processes.

Concluding Remarks

A single applied-field MPD thruster geometry was tested over a wide range of applied-field strengths using three solenoidal magnet geometries. Measurements of discharge voltage, anode power deposition, and plume properties were made in order to assess the dependence of thruster operation on magnetic field shape. It was found that the discharge voltage and anode power deposition depended non-monotonically on the radius of the applied-field magnet, with the largest magnet yielding both the lowest discharge voltage and anode power. The lowest anode power fraction, 66%, was obtained using the intermediate sized magnet with a diameter of 15.2 cm at the highest field strength of 0.14 T. The highest anode power fraction of 80% was obtained using the smallest, 12.7 cm diameter magnet at a field strength of 0.04 T. These results suggest that the thruster performance can be optimized by varying

magnetic-field shape. Langmuir probe measurements of the plume electron density and temperature ranged from 2×10^{18} to 4×10^{18} and from 35,000 to 50,000 K on the centerline, respectively. The centerline electron density decreased with increasing magnet diameter. Electron temperatures decreased with axial distance for all cases. The lowest centerline temperature, 35000 K, was obtained using the 15.2 and 30.4-cm magnet geometries. Preliminary studies of the plasma flux in magnetic field flux tubes indicate that the plasma velocity may be decreasing in the expanding magnetic field. It was not possible to identify the dependence of this behavior on the magnetic field shape. Further investigations of MPD thruster plumes using a wider range of field shapes and strengths and the use of velocity probes are needed to quantify these findings.

References

1. Myers, R.M., Parkes, J.E., and Mantenieks, M.A., "Multimegawatt MPD Thruster Design Considerations," NASA TM 105405, Jan.1992.
2. Seikel, G.R., York, T.M., and Condit, W.C., "Applied-Field Magnetoplasmadynamic Thrusters for Orbit-Raising Missions," Orbit Raising and Manuevering Propulsion: Research Status and Needs, L. Caveny, ed., Prog. in Aeronautics and Astronautics, Vol. 89, American Inst. of Aeronautics and Astronautics, New York, 1984, pp. 260-286.
3. Gerwin, R.A., "Characterization of Plasma Flow Through Magnetic Nozzles," Final Report for Air Force Astronautics Laboratory, Contract No RPL690168, May 1987.
4. Hooper, E.B., "Plasma Detachment from a Magnetic Nozzle,"AIAA Paper 91-2590, June 1991.
5. Kosmahl, H.G., "Three-Dimensional Plasma Acceleration Through Axisymmetric Diverging Magnetic Fields Based On Dipole Moment Approximation," NASA TN D-3782, Jan.1967.
6. Sercel, J.C., "A Simple Model of Plasma Acceleration in a Magnetic Nozzle," AIAA Paper 90-2597, July 1990.

7. York, T.M., Zakrzwski, C., and Soulas, G., "Diagnostics and Performance of a Low-Power MPD Thruster with Applied Magnetic Nozzle," Journal of Propulsion and Power, Vol.9, No.4, July-Aug. 1993, pp. 553-560.

8. Myers. R.M., "Applied-Field MPD Thruster Geometry Effects," AIAA Paper 91-2342, June 1991.

9. Tahara, H., Sasaki, M., Kagaya, Y., and Yoshikawa, T., "Thruster Performance and Acceleration Mechanisms of a Quasi-steady Applied-Field MPD Arcjet," AIAA Paper 90-2554, July 1990.

10. Schoenberg, K., Gerwin, R., Barnes C., Henins, I., Mayo, R., Moses, R., Scarberry, R., and Wurden, G., "Coaxial Plasma Thrusters for High Specific Impulse Propulsion," AIAA Paper 91-3570, Aug. 1991.

11. Myers, R.M., Wehrle, D., Vernyi, M., Biaglow, J., and Reese. S., "A Preliminary Characterization of Applied-Field MPD Thruster Plumes," AIAA Paper, 91-2339, Aug. 1991.

12. Gallimore, A.D., Kelly, A.J., and Jahn, R.G., "Anode Power Deposition in MPD Thrusters," IEPC Paper 91-125, Proceedings of the 22nd Intern. Electric Propulsion Conf., Viareggio, Italy, Oct. 1991.

13. Myers, R.M. and Soulas, G., "Anode Power Deposition in Applied-Field MPD Thrusters," AIAA Paper 92-3463, July 1992.

14. Sovey, J.S. and Mantenieks, M.A., "Performance and Lifetime Assessment of MPD Arc Thruster Technology," Journal of Propulsion and Power, Vol.7, No.1, Jan.-Feb., 1991, pp.71-83.

15. Sovey, J.S., Vetrone R.H., Grisnik, S.P., Myers, R.M., and Parkes, J.E., "Test Facilities for High Power Electric Propulsion,"AIAA Paper 91-3499, Sept.1991.

16. Chung, P.M., Talbot, L., and Touryan, K.J., "Electric Probes in Stationary and Flowing Plasmas: Part 1. Collisionless and Transitional Probes," AIAA Journal, Vol.12, No.2, Feb.1974, pp. 133-154.

17. Swift, J.D. and Schwar, M.J., "Electric Probes for Plasma Diagnostics," American Elsevier Publishing Co., New York, 1970.

18. Myers, R.M., "Scaling of 100 kW Class Applied-Field MPD Thrusters," AIAA Paper 92-3462, July 1992.

19. Moses, R.W., Gerwin, R.A., and Schoenberg, K.F., "Resistive Plasma Detachment in Nozzle Based Coaxial Thrusters," Proceedings from Ninth Symposium, Space Nucl. Power System, Part 3, Albuqerque, N.M., Jan. 1992, pp.1293-1303.
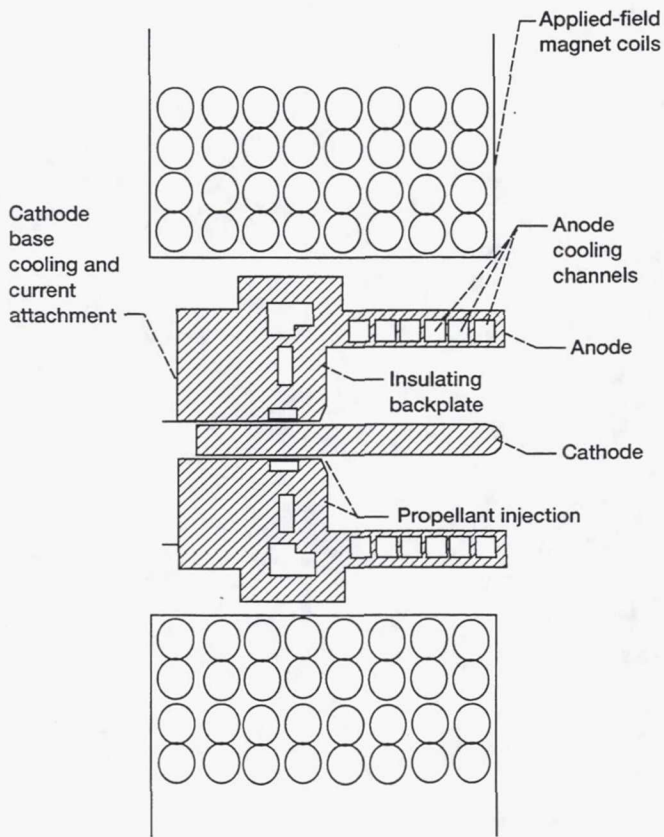
Figure 1.—Applied-field MPD thruster schematic. Anode and cathode length of 7.6-cm. Cathode radius = 0.64-cm, anode radius of 2.54-cm. Thruster exit plane was even with the solenoid exit plane.
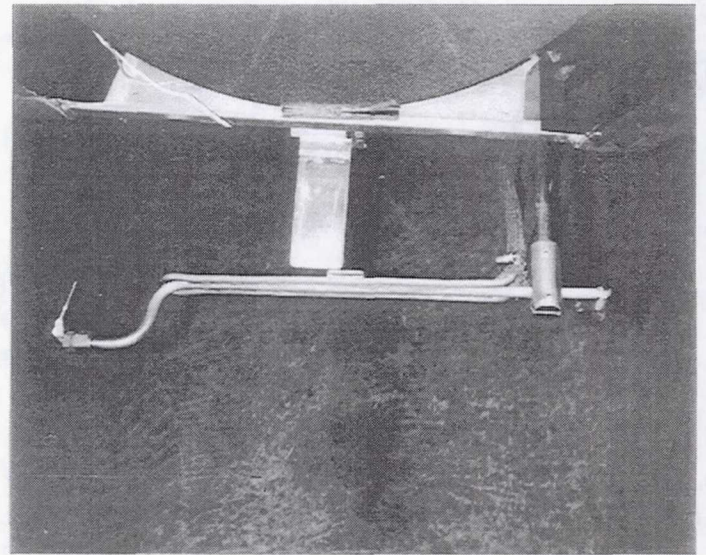
Figure 3.—The water-cooled Langmuir probe arm.
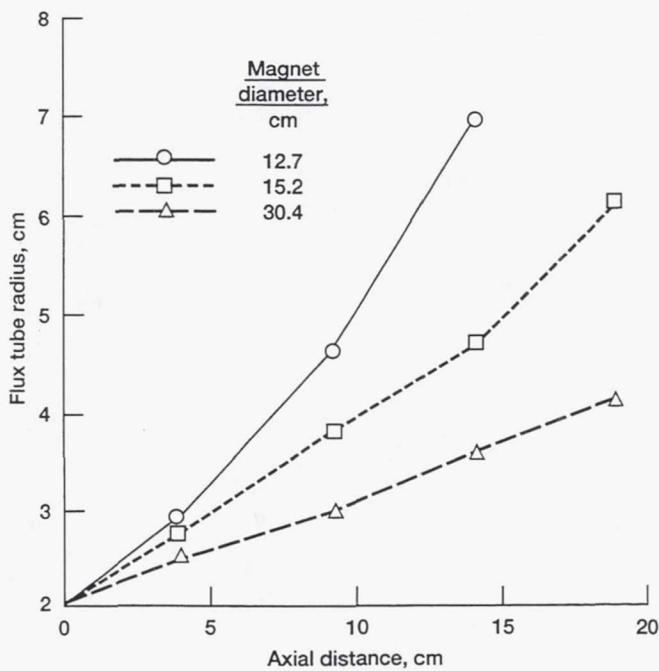
Figure 2.—A plot of the magnetic flux tube radius versus axial distance for all three geometries. Flux tube originates at r = 2.1-cm at the thruster exit plane.
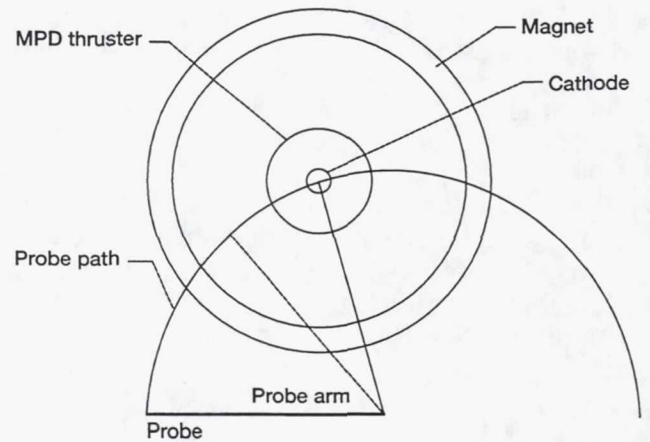
Figure 4.—Geometry of Langmuir probe and MPD system.

8
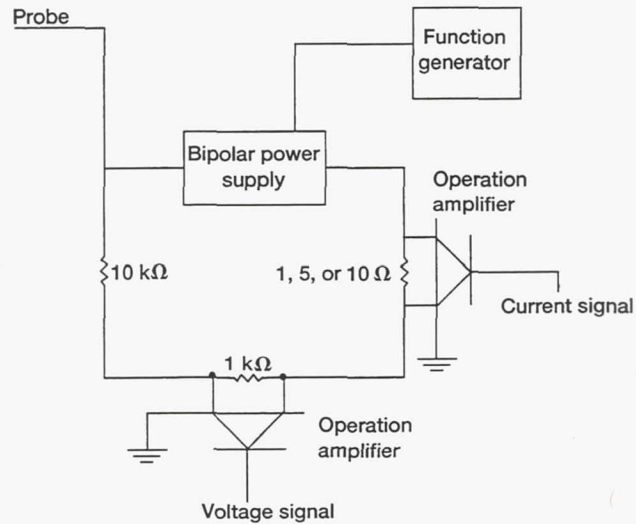
Figure 5.—Single Langmuir probe circuit used to measure I-V characteristics.
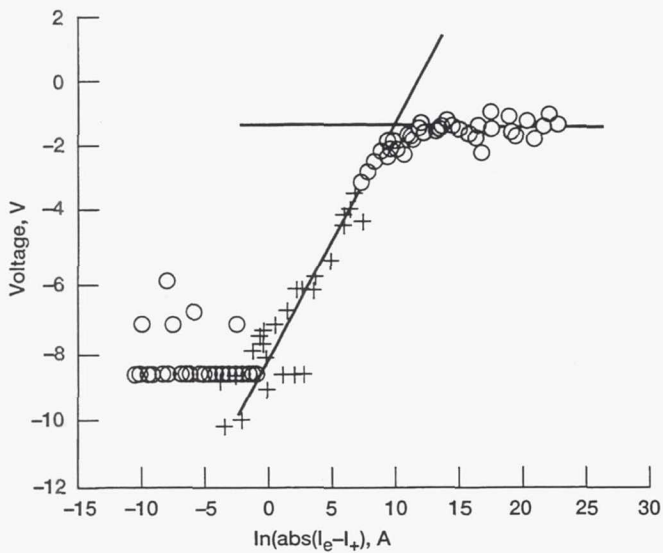
Figure 6.—A plot of the $\ln(abs(I_e{-}I_+))$ versus the probe bias voltage, V. The slope of this curve was used to obtain the electron temperature.
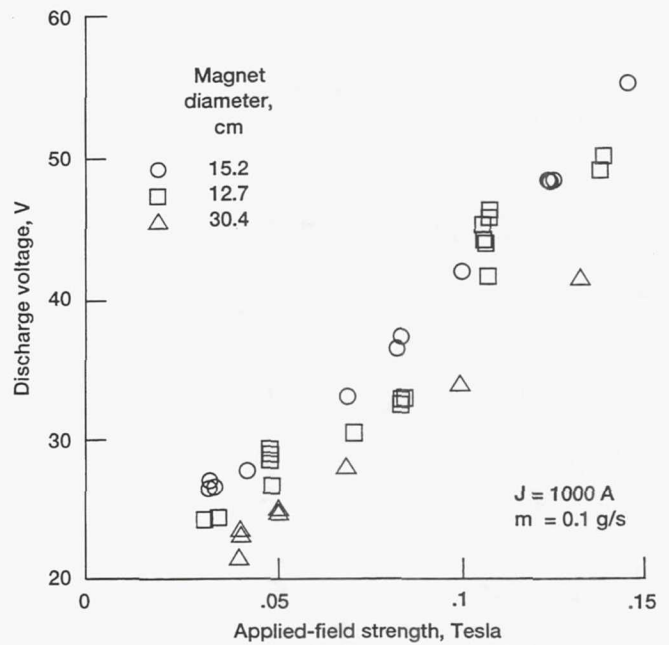
Figure 7.—Discharge voltage versus applied-field strength for each geometry.

Figure 8.—Anode power-fraction versus applied-field strength for all three geometries. J = 1000 A, m = 0.1 g/s. (a) Anode power versus applied-field strength. (b) Anode power-fraction versus applied-field strength.
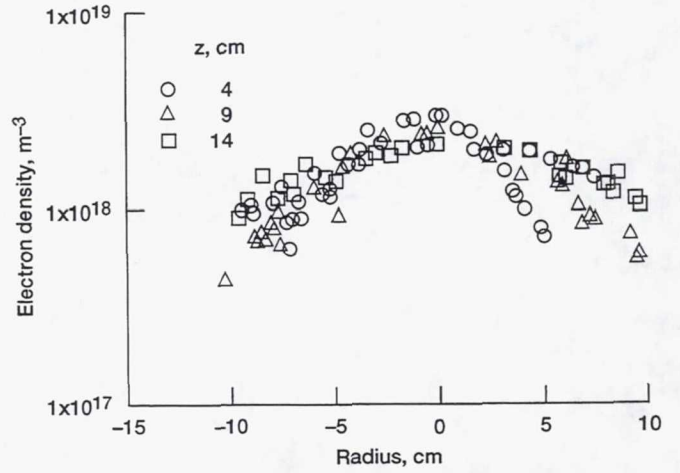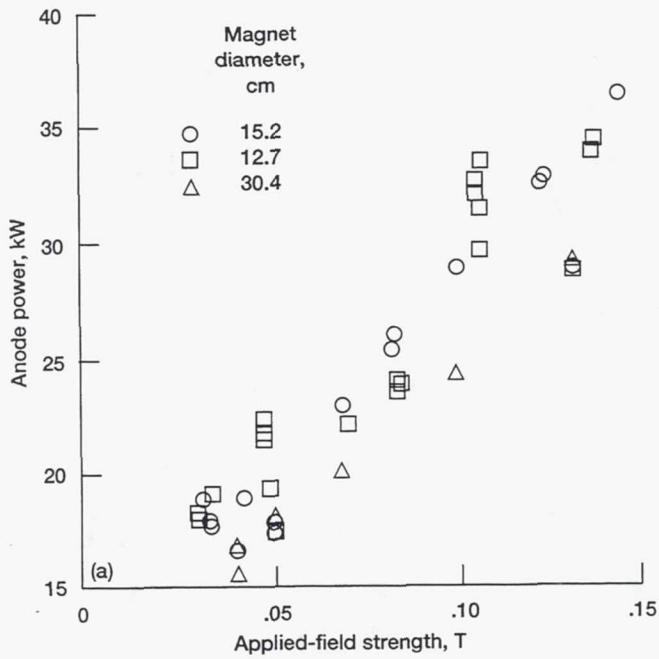
Figure 9.—A plot of the electron density versus radius for the 12.7 -cm magnet geometry at a field strength of 0.14 Tesla and three axial locations.
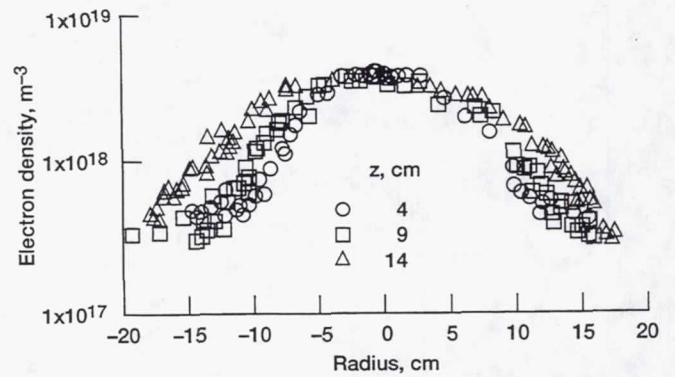

Figure 10.—A plot of the electron density versus radius for the 15.2 -cm magnet geometry at a field strength of 0.04 Tesla and three axial locations.
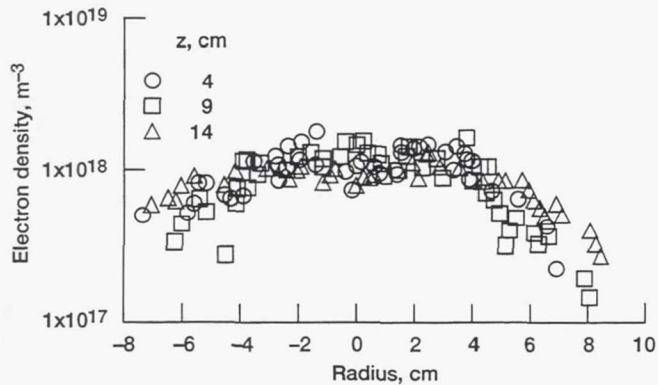
Figure 11.—A plot of the electron density versus radius for the 30.4 -cm magnet geometry at a field strength of 0.04 Tesla and three axial locations.
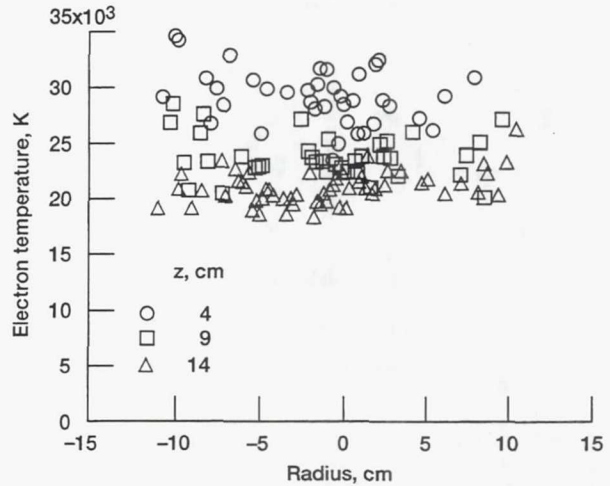
Figure 13.—A plot of the electron temperature versus radius for the 15.2-cm magnet geometry at a filed strength of 0.04 Tesla and three axial locations.
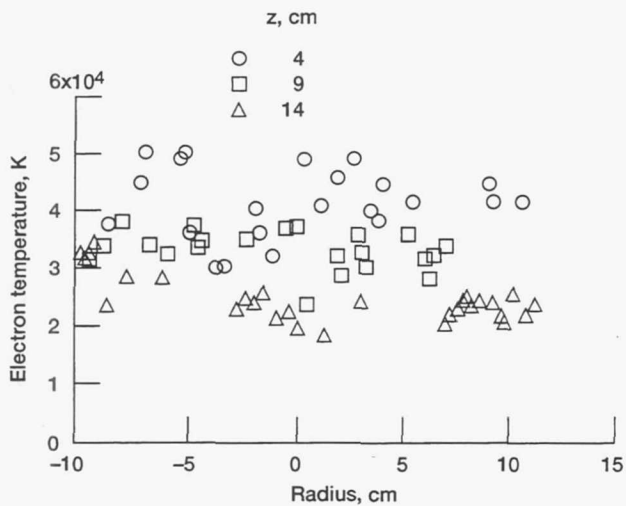
Figure 12.—A plot of the electron temperature versus radius for the 12.7-cm magnet geometry at a field strength of 0.14 Tesla and three axial locations.
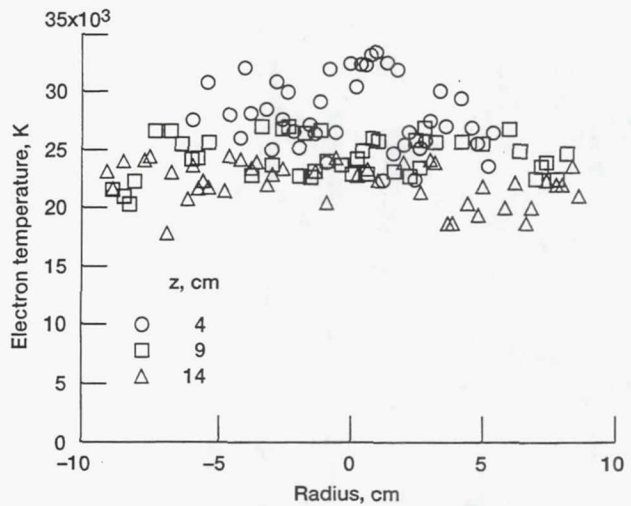
Figure 14.—A plot of the electron temperature versus radius for the 30.4-cm magnet geometry at a field strength of 0.04 Tesla and three axial locations.

11
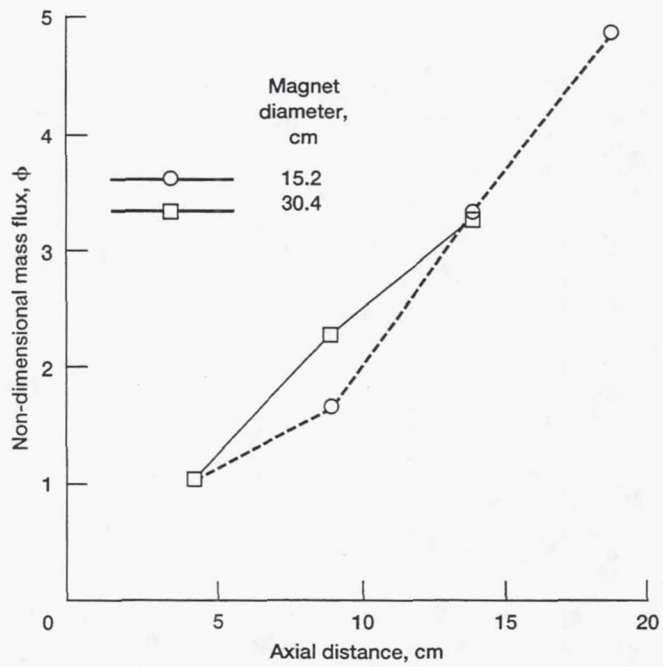
Figure 15.—A plot of the non-dimensional mass flux versus radius for the 15.2 and 30.4-cm geometries at a applied-field strength of 0.04 Tesla.
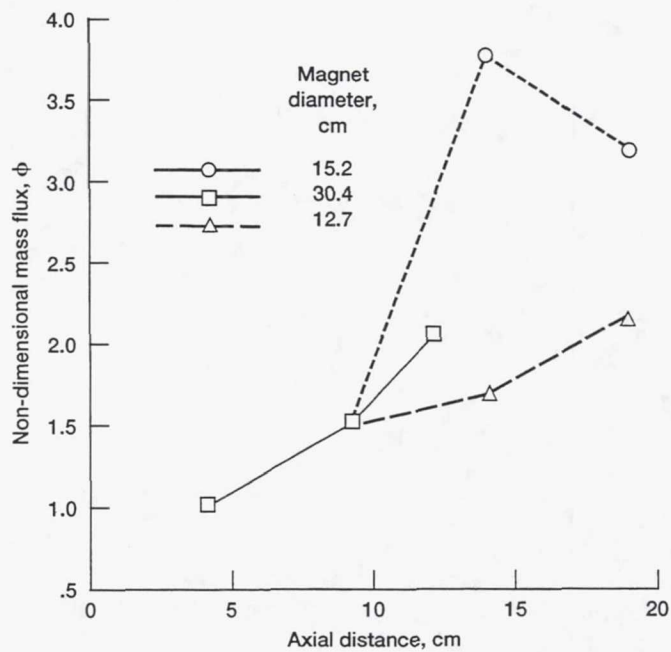
Figure 16.—A plot of the non-dimensional mass flux versus radius for all geometries at a magnetic-field strength of 0.14 Tesla.

REPORT DOCUMENTATION PAGE

1. AGENCY USE ONLY (Leave blank)	2. REPORT DATE	3. REPORT TYPE AND DATES COVERED
	January 1994	Technical Memorandum

4. TITLE AND SUBTITLE

An Investigation of Magnetic Field Effects on Plume Density and Temperature Profiles of an Applied-Field MPD Thruster

6. AUTHOR(S)

S. Ray Bullock and R.M. Myers

5. FUNDING NUMBERS

WU–506–42–31

7. PERFORMING ORGANIZATION NAME(S) AND ADDRESS(ES)

National Aeronautics and Space Administration
Lewis Research Center
Cleveland, Ohio 44135–3191

8. PERFORMING ORGANIZATION REPORT NUMBER

E–8253

9. SPONSORING/MONITORING AGENCY NAME(S) AND ADDRESS(ES)

National Aeronautics and Space Administration
Washington, D.C. 20546–0001

10. SPONSORING/MONITORING AGENCY REPORT NUMBER

NASA TM–106416
IEPC–93–140

12a. DISTRIBUTION/AVAILABILITY STATEMENT

Unclassified - Unlimited
Subject Category 20

12b. DISTRIBUTION CODE

13. ABSTRACT (Maximum 200 words)

Applied-field magnetoplasmadynamic (MPD) thruster performance is below levels required for primary propulsion missions. While MPD thruster performance has been found to increase with the magnitude of the applied-field strength, there is currently little understanding of the impact of applied-field shape on thruster performance. This paper presents the results of a study in which a single applied-field thruster was operated using three solenoidal magnets with diameters of 12.7, 15.2, and 30.4-cm. Thruster voltage and anode power deposition were measured for each applied-field shape over a range of field strengths. Plume electron number density and temperature distributions were measured using a Langmuir probe in an effort to determine the effect of field shape on plume confinement by the diverging magnetic-field for each of the three magnetic field shapes. Results show that the dependence of the measured thruster characteristics on field shape were non-monotonic and that the field shape had a significant effect on the plume density and temperature profiles.

14. SUBJECT TERMS

Electric propulsion; Plasma dynamics; Auxiliary propulsion

15. NUMBER OF PAGES

14

16. PRICE CODE

A03

17. SECURITY CLASSIFICATION OF REPORT	18. SECURITY CLASSIFICATION OF THIS PAGE	19. SECURITY CLASSIFICATION OF ABSTRACT	20. LIMITATION OF ABSTRACT
Unclassified	Unclassified	Unclassified	